NANO LETTERS

pubs.acs.org/NanoLett

Plasmonic Response of Nanoscale Spirals

Jed I. Ziegler* and Richard F. Haglund, Jr.

Department of Physics and Astronomy, Vanderbilt University, Nashville, Tennessee 37235-1807

ABSTRACT The Archimedean spiral geometry presents a platform for exploration of complex plasmonic mechanisms and applications. Here we show both through simulations and experiment that more complex plasmonic modes with unique near-field structure and larger mode volumes can be realized within a single, topologically robust structure. In the spiral, complex polarization response, resonant interactions and symmetry-breaking features are defined by the width and spacing of the spiral tracks and by the winding number of the spiral.

KEYWORDS Nanospiral, broad band absorber, nanomanipulator, nonlinear near-field structure

Studies of localized surface plasmons in complex configurations have up to now been focused on ensembles or composite structures. Complex plasmonic responses in nanoscale structures have been generated either through through mode hybridization[1] in heterogeneous structures such as nanostars,[2] nanotriangles,[3] and ring-disk systems,[4,5] or by breaking topological symmetries in such a way that high-order modes are pumped.[6−8] These structures are inherently limited to a small number of simple oscillatory patterns defined by the incident polarization.

Here we show, both through simulations and experiments, that an entirely different class of plasmonic structures characterized by a large number of distinct, complex plasmonic modes can be realized within a single, topologically robust structure: the spiral. In the spiral, complex polarization response, resonant interactions, and symmetry-breaking features are defined by the width and spacing of the spiral tracks and by the winding number of the spiral. In previous work with the spiral geometry, intraparticle interactions, and thus plasmonic complexity, was limited due to relatively large arm widths and spacings;[9−11] spirals with larger winding numbers likewise tend to be dominated by a single resonant mode.[12,13] In contrast, we focus here on compact, nanoscale Archimedean spirals as a model plasmonic system. The absence of symmetry coupled with a spatially compact geometry ensures that these plasmonic nanospirals exhibit a large system of modes populated by unique near-field configurations at spectrally distinct locations.

Our model plasmonic nanostructures are spirals with subwavelength dimensions (Figure 1a) thereby confining all plasmonic activity to the near-field region. We focus on spirals with winding numbers between 1 and 2 (2π and 4π) in which emergent properties are manifest in complex intraparticle interactions. Using scanning electron micrographs and measured spectra, we simulated the optical response with finite-difference time-domain (FDTD) simulation software (Lumerical) to investigate the near-field interactions and mode structure observed in experiment. We first focused on lithographically produced arrays of 4π spirals: 20 nm thick Au spirals with a 650 nm grating constant on a SiO_2 substrate covered with 27 nm of ITO, the latter measured by white-light ellipsometry. The dielectric properties of the ITO were derived from these ellipsometric measurements, extrapolating as necessary beyond the 900 nm cutoff of the ellipsometer. The FDTD calculation simulates a single spiral with periodic boundary conditions and an *x*-polarized, 2 fs, white-light pulse that spanned the spectral region 400 to 1400 nm, reflecting the spectral range of our experiments. (See Supporting Information for complete description of experimental procedure.)

Using the 4π spiral (Figure 1a) as a model, Figure 1b−d displays examples of three structures that are characteristic of the spiral response at any winding number: a radially oriented "hourglass" mode (Figure 1b); a standing-wave mode (Figure 1d) analogous to longitudinal modes of a

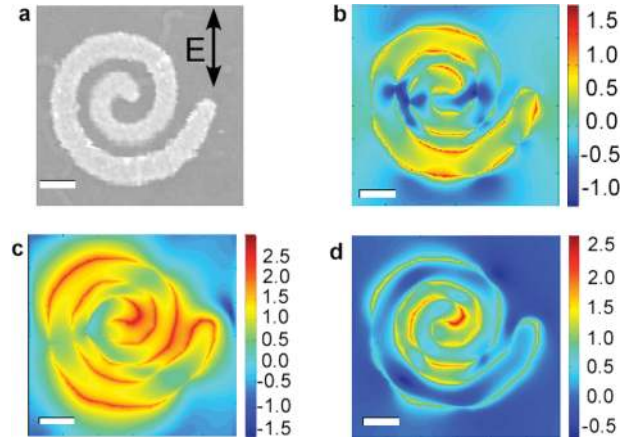

FIGURE 1. (a) Micrograph of the experimentally produced 4π spiral used as the model in simulation and examples of the near-field distribution of each mode configuration for the 4π spiral; (b) hourglass (601 nm), (c) focusing (847 nm), and (d) standing-wave (1233 nm). Scale bar is 100 nm wide and the color bar is scaled to $\log_{10}$ (normalized transmission).

* To whom correspondence should be addressed. E-mail: jed.i.ziegler@vanderbilt.edu.

Received for review: 04/26/2010
Published on Web: 07/26/2010

DOI: 10.1021/nl101475n | *Nano Lett.* **2010,** *10,* 3013–3018

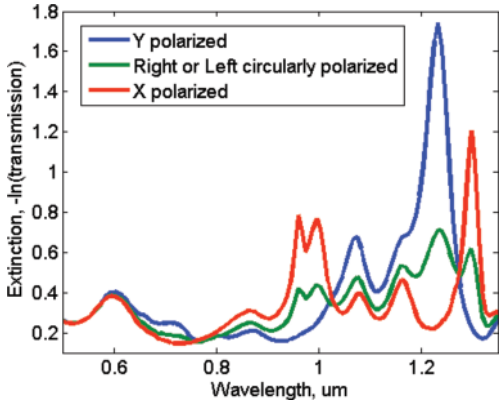

FIGURE 2. Simulated extinction spectra for a 4π spiral illuminated by incident polarizations oriented on the *X*- and *Y*-axis as well as right-hand circularly polarized. Left and right-handed polarizations produce the same spectral features at almost the same intensities.

nanorod[14,15] and a focusing mode (Figure 1c) that centers the majority of the confined energy at either or both ends of the spiral. Analysis of the dominant extinction mechanism, e.g., absorption or radiative damping, within the spectral regions of each configuration illustrated a mild preference of roughly a factor of 2 for radiative damping in all but the standing-wave configuration, where the mechanisms contributed equally. The lack of a clear dominant mechanism suggests a complex geometric origin of the mode structure and contributes to the nonzero extinction found under each resonant mode across the entire spectral region. Remarkably, even when excited by linearly polarized light, the spiral exhibits a robust population of modes, spatially selective field enhancements, and a tunable spectral response. Initial investigations with circular polarizations actually suggest that superposition of the *x*- and *y*-linear mode structure describes the circular mode structure, regardless of the circular orientation of the near-field structure of the linear modes, as illustrated in Figure 2. The unique behavior of these modes suggests applications in plasmonic focusing, nanoscale manipulation of dielectric objects,[16] chiral interactions, and enhanced chemical and optical processes such as surface-enhanced Raman scattering (SERS) and second-harmonic generation.

The correlation between spectral features and winding number allows us to generate and control the number, intensity, and spectral position of the resonant modes. This tunability is illustrated in Figure 3 wherein the spectral elements of simulated spirals, based on electron micrographs of experimentally produced spirals, evolve from 2π to 4π in one-eighth π-steps. This structural evolution was generated by editing the micrograph such that the exact geometry of the spiral, including any variations in arm width or spacing as well as the distinct end geometry of the spiral arm, remained unchanged as the arm length was decreased so as to isolate the spectral dependence on winding number. A definite structure in mode organization becomes apparent

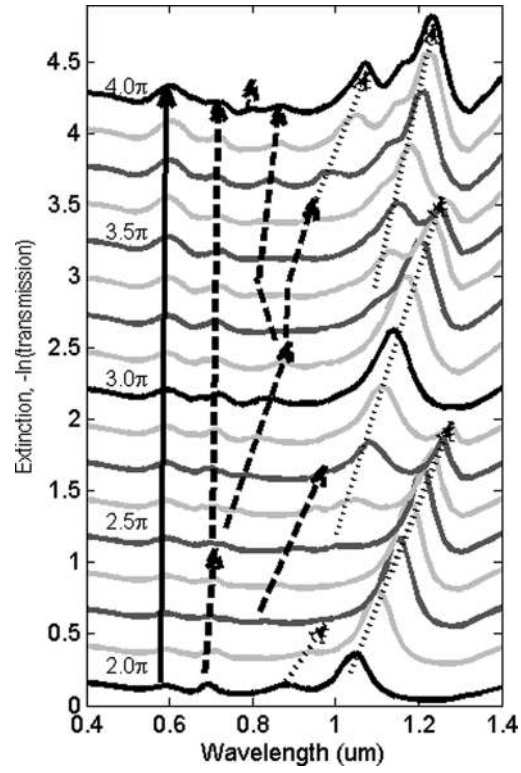

FIGURE 3. Simulated extinction spectra of spirals with winding numbers evolving from 2 to 4π in steps of $\pi/8$. The evolution of each mode is marked with arrows, solid arrow for the hourglass mode, the dashed arrow for the focusing mode, and dotted arrows for standing modes. The offset waterfall is 2.5.

in which the near-field response of each configuration (hourglass, standing-wave, and focusing) is associated with specific spectral locations as the spiral evolves in winding number. We refer to these specific spectral features as "elements." For the spiral parameters chosen in these experiments, there are ten such elements, as shown in Figure 3.

Given this large set of distinct mode structures, it is tempting to use quantitative figures of merit to characterize the system. The quality factor, *Q*, and the effective mode area, A_{eff}, that together describe the efficiency of a resonator system were calculated for each mode configuration from the simulation and experimental data. The *Q*-factor for modes of the 4π spiral were all found to be rather low and relatively close together, between 8 and 35. Considering the notable variation in lateral dimensions between 2 and 4π, we analyzed the A_{eff} of each element as the winding number grew (Figure 4). We found that each element has its own distinct progression but the focusing and standing-wave configurations vary within the same values without any clearly distinguished regions. To this end, analysis of the individual modes using the *Q*-factor or A_{eff} fails to capture the unique aspects of the different configurations. Thus a phenomenological analysis is in fact more informative.

The "hourglass" configuration (solid line in Figure 3) is found at the shortest wavelength, around 580 nm, and is

DOI: 10.1021/nl101475n | *Nano Lett.* **2010,** *10,* 3013–3018

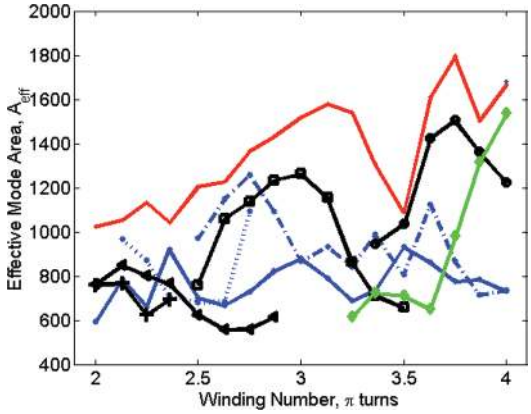

FIGURE 4. Linear plot of the effective mode area, as a function of winding number, for each element from Figure 2: the hourglass mode (solid red line), the three distinguishable focusing modes (blue lines), the four standing-wave modes (solid black lines), and the mode that transitions from focusing to standing-wave (solid green line). The dimensionless quantity, A_{eff}, is equal to the max field enhancement divided by the summed enhancement over the entire monitor area.

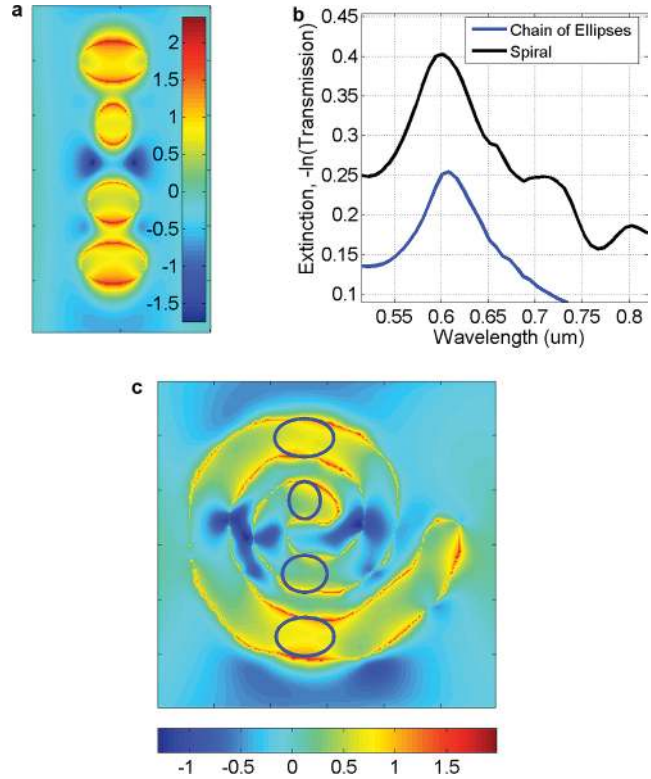

FIGURE 5. (a) Near-field distribution of a chain of ellipses matched to regions of field enhancement on the hourglass configuration for the 4π spiral. (b) Comparison of the spectral position of the hourglass configuration and the chain of ellipses. (c) Near-field distribution of the hourglass configuration with overlay of the chain of ellipses.

independent of winding number, shifting no more than a few tens of nanometers as arm spacing or width is varied. The hourglass orientation also tracks the polarization of the incident light wave without changing either spectral position or spatial orientation. The mode energy is localized by direct coupling between neighboring azimuthal sections of the spiral arm oriented parallel to the incident polarization, similar to the characteristic transverse mode generated by lines of nanodisks.[17] Indeed, simulations of the plasmonic responses of ellipses with their long axes perpendicular to the electric-field polarization, overlapped the hourglass configuration (Figure 5). This mechanism of energy localization is defined spectrally by the average diameter of the ellipses parallel to the line of structures. The resonance frequency is stabilized against aberrations within the ensemble by near-field coupling, acting as strongly coupled dipole oscillators whose resonances are locked by longer range coupling across the entire ensemble.[18] Thus the hourglass mode is unique both in its spectral and near-field stability and the fact that the mechanism for its generation arises from an ensemble of independent subregions within the spiral.

The standing-wave configuration (dotted lines in Figure 3) exhibits a plasmonic response resembling the harmonic modes of nanorods with high aspect ratios. In the spiral geometry, one can view the nanorod as being bent along the spiral arm; this distortion reorganizes the relative field intensities such that the enhancement at the ends is larger than, but within a factor of 10 of, the maxima along the arm. Computational comparisons of the nanorod and spiral modes, not shown here, suggest that the standing-wave modes are slightly red shifted from the analogous nanorod modes in the spectral region beyond 875 nm. Such an effect is expected, since the complexity of the reconfiguration would increase the radiative dampening as the modes bend to follow the spiral. In the standing-wave configuration, the spiral modes have significantly higher field intensities than the analogous nanorod modes, which presented maximum localized enhancement factor of 76 compared to 1317 for the analogous spiral mode of a 4π spiral. Moreover, these modes grow from the background or from the weaker focusing configuration and collapse around 1300 nm whereas the nanorod only adds harmonic modes without the loss of lower-order harmonics.

In Figure 3, the standing-wave region of the plasmonic spectrum contains five elements that form, redshift through an intensity maximum, and then dissipate into the baseline as winding number increases. As the winding number increases, each of these five elements exhibits unique variations in the number of maxima, evolution of the maximum field enhancement, and azimuthal distribution of local field enhancements generated by the self-interactions of the spiral. For plasmonic applications, these elements retain the positive attributes of the numerous, spatially extended nanorod modes, but add higher localized field intensities, a chiral structure, and multiple, spectrally tunable elements as the spiral evolves. Of all the mode configurations, the strongest local field enhancements are produced by the standing-wave. However, it is also the most variegated of the configurations with the magnitude of the maximum local enhancement varying by greater than a factor of 13, as the

DOI: 10.1021/nl101475n | *Nano Lett.* **2010,** *10,* 3013–3018

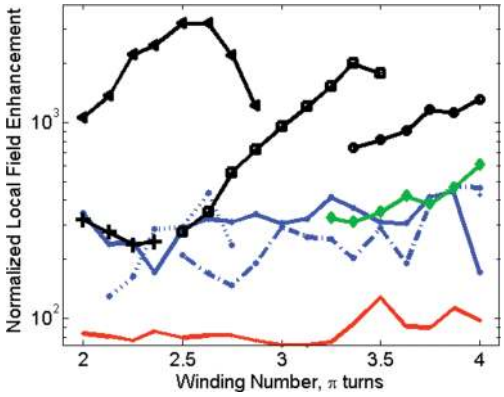

FIGURE 6. Logarithmic plot of the maximum local field enhancement within a single 2 × 2 × 2 nm pixel, as a function of winding number, for each element from Figure 2: the hourglass mode (solid red line), the three distinguishable focusing modes (blue lines), the four standing-wave modes (solid black lines), and the mode that transitions from focusing to standing-wave (solid green line).

winding number is tuned. This variation and comparison with the other configurations is presented in Figure 6. The exceptional field enhancements in this configuration suggest that these could be used to generate a SERS signal over a broad spatial region or as a collecting mode that could attract dielectric particles into specific locations within the spiral with unique near-field configurations.

Finally, the focusing configuration (dashed line in Figure 3) is completely defined by the spiral geometry and has no obvious analog to simpler plasmonic structures. Some plasmonic focusing geometries use sharpened points (triangle/bowtie[19]), Fresnel lenses,[20] or self-similar chains of nanospheres[21] to generate a single focusing mode. On the other hand, the nanospiral focuses the near-field energy into standing wave maxima along the spiral arm that increase in total confined energy as they approach the center. The number of standing-wave maxima, as well as the degree of localization in the arm sections that are closer to the center of the field enhancement, varies depending on the specific resonant wavelength and the geometric parameters of the spiral. Figure 1d presents an example where the maximum enhancements are contained in a 2π region at the center, though this region can be longer. It should be noted that the evolution of the near-field distribution as the linear polarization is rotated suggests that the focusing configuration is not a superposition of the other two configurations.

Focusing modes are confined to a spectral region between the hourglass mode and approximately 900 nm. There is a transition region between focusing and standing-wave configurations above 900 nm where confined energy is redistributed within the local maxima until the mode is clearly configured as a standing-wave at 1000 nm. Higher harmonics analogous to those of nanorods do exist within this region, but the comprehensive reorganization of confined energy makes such a comparison uninformative. This configuration suggests interesting applications utilizing the inwardly oriented electric-field gradient for simultaneous self-focusing and Raman enhancement of molecules in the local environment, as well as enhancement of optically chiral interactions.

Geometrically, the tuning characteristics of a single spiral configuration as a function of winding number are sensitive to fabrication errors in the width and spacing of the spiral arms, including local protrusions or variations of the arm spacing to width ratio. This highlights two sources of disruption to the plasmonic structure. One is from local protrusions that would cause two azimuthally neighboring arm sections to couple together more strongly, giving preference to a localized resonant mode that is not attributable to the spiral geometry. If such a coupling was strong enough to be disruptive to characteristic modes, we would expect a significant reorganization of the positions and relative intensities of the resonant structure compared to other spirals with similar geometric parameters. This was not observed either within a single array or between arrays of similar production parameters. The second source of disruption can arise from variation of the arm width and spacing if the mechanisms that define the structure of each configuration are directly defined by these values, as opposed to the overall geometry. This would dramatically increase the sensitivity of the nanospiral properties to small defects that are inevitable in these topologically complex structures that would, in turn, render the spiral unsatisfactory for applications and too irreproducible for fundamental plasmonic investigations. To verify experimentally that nanoscale spirals would retain their distinct plasmonic characteristics, we measured the plasmonic response of nanospirals with width and/or spacing variations smaller than ±30 nm from the average design value. These limits are defined by the scale of the total structure, outside these parameters the spiral arm either becomes too thin and fractures or is the approximate limit of feature sizes for the lithographic techniques used.

We found that changes that result in significantly larger lateral dimensions tended to redshift modes above 600 nm, compared with laterally smaller spirals with new focusing modes appearing between the relatively stationary hourglass mode and the longer-wavelength modes. This is illustrated for the 2π spiral in Figure 7a where the lateral diameter at the widest point is varied between 180 and 240 nm. For smaller changes, we were able to distinguish the boundaries between regions that are strongly vs weakly affected by tuning arm spacing and width, as illustrated in Figure 7b,c for the 3π spiral. The hourglass mode and standing-wave modes above 1000 nm experience minimal spectral shifts, ± 20 nm and ±30 nm, respectively, though significant changes in the relative intensities can occur as energy is redistributed among the evolving elements. The hourglass mode is the least dependent on small changes to the nonwinding parameters as it is does not disappear and experiences minor

DOI: 10.1021/nl101475n | *Nano Lett.* **2010,** *10,* 3013–3018

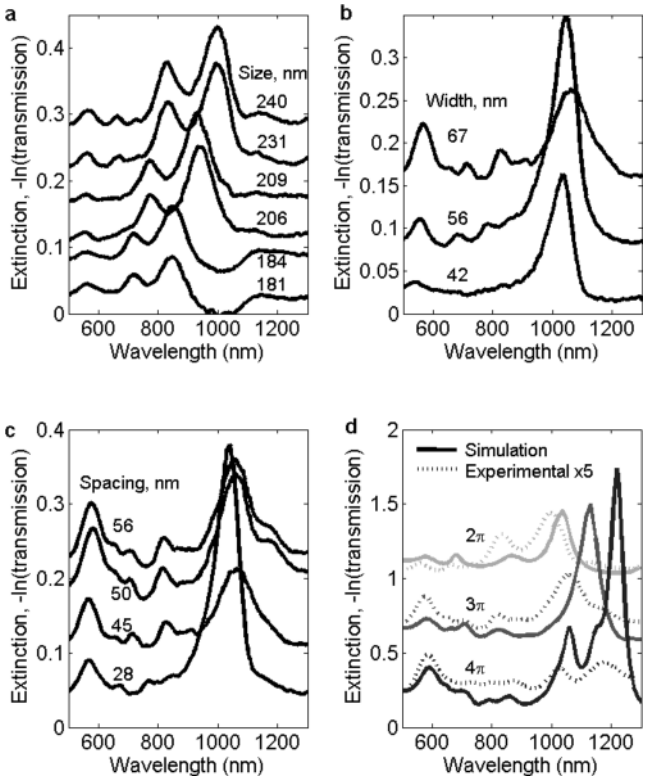

FIGURE 7. Experimentally measured extinction spectra of (a) 2π spirals with arm spacing increasing vertically, (b) 3π spirals with arm spacing increasing vertically, and (c) 3π spirals with arm width increasing vertically. (d) Simulated extinction spectrum and experimental extinction spectrum scaled by a factor of 5 for the 2, 3, and 4π spiral. Mismatches between the long-wavelength peaks are explained in the methods section.

spectral shifts (± 20 nm), although its relative intensity can vary significantly as shown in Figure 7b. The standing-wave configuration is much more tunable than the others with certain parameters that optimize extinction intensity and is more dependent on winding number to define the extent to which each element shifts or if it decays. Comparison of the 3π and 4π spirals, considering that the standing-wave element in the 3π spiral is in the middle of its evolution while at 4π the longest wavelength element is at the end of its tuning range, showed that the spectral position of the 3π standing-wave mode is stable against changes in nonwinding parameters while the 4π standing-wave modes are more transient and spectrally mobile. This suggests that any transient behavior of the standing-wave mode is a result of its proximity to the end of its tuning cycle. The focusing modes are strongly affected by tuning, as the modes will easily disappear or sporadically form or strongly shift. These shifts are significant enough that different elements can overlap so the extent of the shifts is not clear but the spectral region of this activity is defined by the focusing configuration. Thus, although the exact distribution may vary, the general focusing structure should persist. These initial experimental attempts lead us to conclude that although the spiral is sensitive to the arm width and spacing, the resonant structure of the three configurations, and the dependence of plasmonic response on winding number, are robust.

Thus we argue that the promise of the spiral geometry observed in the simulations is validated by experiment. The Archimedean spiral presents a nanostructure that is complex but contains the components of a useful and practical plasmonic toolbox: independently variable spectral elements together with regions of clearly identifiable near-field plasmonic field enhancements. The spiral supports a significant number of resonant elements that self-organize into regions that are calculable from geometric features of the spiral geometry, are spectrally tunable via the winding number, and remain reasonably stable under lithographic variations in arm width and spacing. Furthermore, the specific near-field structures that operate over the same spatial regions and adjacent spectral regions, allow for versatile manipulation of the time-varying surface charge distributions. For fundamental plasmonic research, the spiral is a single particle laboratory for exploring complex intraparticle interactions between modes and substructures compressed into adjacent near-field regions. For applications, the subwavelength spiral is large enough to be a substrate for molecular and biological interactions in which the electronic properties of subregions can be spectrally modulated as defined by the near-field topography of each mode. This makes the spiral geometry an ideal platform for advanced application such as a molecular manipulator or trap incorporating orientational specificity or focusing in a surface-enhanced Raman structure.

Acknowledgment. This research was supported by the Office of Science, U.S. Department of Energy (DE-FG02-01ER45916).

Supporting Information Available. A method section describing the computational setup and experimental fabrication of the nanospirals. This material is available free of charge via the Internet at http://pubs.acs.org.

REFERENCES AND NOTES

(1) Prodan, E.; Radloff, C.; Halas, N. J.; Nordlander, P. *Science* **2003**, *302*, 419–422.
(2) Hao, F.; Nehl, C. L.; Hafner, J. H.; Nordlander, P. *Nano Lett.* **2007**, *7*, 729–732.
(3) Archermann, M.; Shuford, K. L.; Schatz, G. C.; Dahanayaka, D. H.; Bumm, L. A.; Klimov, V. I. *Opt. Lett.* **2007**, *32*, 2254–2256.
(4) Hao, F.; Nordlander, P.; Burnett, M. T.; Maier, S. A. *Phys. Rev. B* **2007**, *76*, 245417.
(5) Wu, Y.; Nordlander, P. *J. Chem. Phys.* **2006**, *125*, 124708.
(6) Mirin, N. A.; Bao, B.; Nordlander, P. *J. Phys. Chem. A* **2009**, *113*, 4028–4034.
(7) Brandl, D. W.; Mirin, N. A.; Nordlander, P. *J. Phys. Chem. B* **2006**, *110*, 12302–12310.
(8) Hao, F.; Larsson, E. M.; Ali, T. A.; Sutherland, D. S.; Nordlander, P. *Chem. Phys. Lett.* **2008**, *458*, 262–266.
(9) Yang, S.; Chen, W.; Nelson, R. L.; Zhan, Q. *Opt. Lett.* **2009**, *34*, 30473049.

DOI: 10.1021/nl101475n | *Nano Lett.* **2010,** *10,* 3013–3018

(10) Chen, W.; Abeysinghe, D. C.; Nelson, R. L.; Zhan, Q. *Nano Lett.* **2010**, *10* (6), 2075–2079.
(11) Gorodetski, Y.; Niv, A.; Kleiner, V.; Hasman, E. *Phys. Rev. Lett.* **2008**, *101*, No. 043903.
(12) Ohno, T.; Miyanishi, S. *Opt. Express* **2006**, *14*, 6285–6290.
(13) Drezet, A.; Genet, C.; Laluet, J.; Ebbesen, T. W. *Opt. Express* **2008**, *16*, 12559–12570.
(14) Krenn, J. R.; et al. *APL* **2000**, *77*, 3379–3381.
(15) Okamoto, H.; Imura, K. *J. Mater. Chem.* **2006**, *16*, 3920–3928.
(16) Righini, M.; Volpe, G.; Girard, C.; Petrov, D.; Quidant, R. *Phys. Rev. Lett.* **2008**, *100*, 186804.
(17) Zou, S.; Janel, N.; Schatz, G. C. *J. Chem. Phys.* **2004**, *120*, 10871–10875.
(18) Maier, S. A.; Kik, P. G.; Atwater, H. A. *Appl. Phys. Lett.* **2002**, *81*, 1714–1716.
(19) Jiao, X.; Goeckeritz, J.; Blair, S.; Oldman, M. *Plasmonics* **2009**, *4*, 37–50.
(20) Smolyaninov, I. I.; Hung, Y.; Davis, C. C. *Phys. Rev. B* **2007**, *76*, 205424.
(21) Li, K.; Stockman, M. I.; Bergman, D. *J. Phys. Rev. Lett.* **2003**, *91*, 22740.

DOI: 10.1021/nl101475n | *Nano Lett.* **2010,** *10,* 3013–-3018